



Beneficial Effects of Theta-Burst Transcranial Magnetic Stimulation on Stroke Injury via Improving Neuronal Microenvironment and Mitochondrial Integrity

Xuemei Zong^{1,2} · Yan Dong² · Yuyu Li¹ · Luodan Yang² · Yong Li² · Baocheng Yang^{1,2} · Lorelei Tucker² · Ningjun Zhao¹ · Darrell W. Brann² · Xianliang Yan¹ · Shuqun Hu¹ · Quanguang Zhang²

Received: 9 June 2019 / Revised: 19 August 2019 / Accepted: 21 August 2019 / Published online: 12 September 2019
© Springer Science+Business Media, LLC, part of Springer Nature 2019

Abstract

Recent work suggests that repetitive transcranial magnetic stimulation (rTMS) may beneficially alter the pathological status of several neurological disorders, although the mechanism remains unclear. The current study was designed to investigate the effects of rTMS on behavioral deficits and potential underlying mechanisms in a rat photothrombotic (PT) stroke model. From day 0 (3 h) to day 5 after the establishment of PT stroke, 5-min daily continuous theta-burst rTMS (3 pulses of 50 Hz repeated every 200 ms, intensity at 200 G) was applied on the infarct hemisphere. We report that rTMS significantly attenuated behavioral deficits and infarct volume after PT stroke. Further investigation demonstrated that rTMS remarkably reduced synaptic loss and neuronal degeneration in the peri-infarct cortical region. Mechanistic studies displayed that beneficial effects of rTMS were associated with robust suppression of reactive micro/astrogliosis and the overproduction of pro-inflammatory cytokines, as well as oxidative stress and oxidative neuronal damage especially at the late stage following PT stroke. Intriguingly, rTMS could effectively induce a shift in microglial M1/M2 phenotype activation and an A1 to A2 switch in astrocytic phenotypes. In addition, the release of anti-inflammatory cytokines and mitochondrial MnSOD in peri-infarct regions were elevated following rTMS treatment. Finally, rTMS treatment efficaciously preserved mitochondrial membrane integrity and suppressed the intrinsic mitochondrial caspase-9/3 apoptotic pathway within the peri-infarct cortex. Our novel findings indicate that rTMS treatment exerted robust neuroprotection when applied at least 3 h after ischemic stroke. The underlying mechanisms are partially associated with improvement of the local neuronal microenvironment by altering inflammatory and oxidative status and preserving mitochondrial integrity in the peri-infarct zone. These findings provide strong support for the promising therapeutic effect of rTMS against ischemic neuronal injury and functional deficits following stroke.

Keywords Ischemic stroke · Functional recovery · Neuroprotection · Neuroinflammation · Oxidative stress · Apoptosis

Xuemei Zong and Yan Dong contributed equally to this work.

✉ Shuqun Hu
hushuqun88@126.com

✉ Quanguang Zhang
qzhang@augusta.edu

¹ Jiangsu Provincial Institute of Health Emergency, Xuzhou Medical University; the Emergency Center of the Affiliated Hospital of Xuzhou Medical University, Xuzhou 221002, Jiangsu province, China

² Department of Neuroscience and Regenerative Medicine, Medical College of Georgia, Augusta University, 1120 15th Street, Augusta, GA 30912, USA

Introduction

Ischemic stroke is a leading cause of death and disability, with nearly 800,000 new cases each year in the USA alone, disproportionately affecting older people [1]. Currently, treatment options are limited to two approved treatments, thrombolysis via tPA and mechanical thrombectomy [2, 3]. As such, new treatments must be developed to expand the toolbox available to clinicians. Ischemic stroke commences with the reduction or cessation of blood flow to a region of brain due to occlusion of cerebral vasculature, leading to oxygen deprivation and cell death in the occluded area if reperfusion does not occur within 4.5 h [3–5]. Upon reperfusion, mitochondria generate

excessive reactive oxygen species that damage cellular macromolecules [4]. Meanwhile, glial cells activate to release inflammatory cytokines and form scarring around the infarct core, a region characterized by necrotic cell death [6]. Surrounding the infarct core is an area of at-risk tissue called the penumbra, a salvageable region that represents a primary target of stroke research [7, 8].

Recent work has highlighted the importance of the neuronal microenvironment in recovery in stroke and other forms of ischemic brain injury [9–11]. In particular, glial activation, inflammation, and oxidative stress are key factors that contribute to the final outcome of tissue in the penumbra [9, 11]. Our work and others demonstrated that long-term neuroinflammatory over-activation after stroke can impede the repair process and compound neural degeneration and cell death, and that targeting this response can be neuroprotective [12–14].

Microglia, the resident macrophage of the brain, are early contributors to neuroinflammation after brain injury and play a crucial role in the post-stroke recovery phase [15, 16]. Upon activation, microglia polarize to one of two phenotypes, the pro-inflammatory M1 and the anti-inflammatory M2 [17]. Shifting the balance of polarization towards the M2 phenotype has been demonstrated to be neuroprotective in different animal models of ischemic stroke [12, 18, 19]. Much like microglia, astrocytes also transition to one of two polarized phenotypes after activation by ischemic brain injury, the neurotoxic A1 and the neuroprotective A2 [20, 21]. Upon activation, astrocytes play a pivotal role in the post-injury response, releasing inflammatory cytokines, secreting neurotrophic factors, and forming a glial scar around damaged tissue, which simultaneously sequesters damaging necrotic debris and hampers reparative processes [21, 22]. Treatments that promote the A2 phenotype may improve outcomes after stroke, a hypothesis tested in this study.

Mitochondrial integrity after stroke is also a key factor in the outcome of salvageable tissue and neurological function [4]. After ischemic insult, mitochondrial components are compromised, causing the generation of reactive oxygen species that perpetuate long-term dysfunction via damage to key cellular macromolecules [4]. Treatments that can preserve or restore mitochondrial dysfunction have been beneficial in animal models of stroke, neurodegenerative conditions, and ischemic brain injury [12, 23–29]. Oxidative damage after ischemic insult can act through a number of pathways to induce apoptotic cell death [4]. All of these factors compound one another, and as such, targeting the neuronal environment may be a viable strategy in preventing cell death in the salvageable penumbra and promoting repair processes that may improve recovery after stroke. Transcranial magnetic stimulation (TMS) may be one potential therapy to achieve this.

TMS is the application of a targeted external magnetic field to the brain, inducing an electric current within a

selected region of the brain [30]. This induced current can inhibit neural activity at lower frequencies and can stimulate activity at higher frequencies [31]. Repeated TMS (rTMS) has demonstrated efficacy in treating psychiatric disorders like depression and obsessive-compulsive disorder, as well as some neurological conditions such as Parkinson's disease (PD) [30, 32, 33]. rTMS has been applied to several injury and disease animal models, revealing many beneficial behavioral and neuroprotective effects [34, 35]. Application of rTMS after an experimental stroke model increased expression of genes involved in neural remodeling, repair, neuroprotection, and injury response [36]. In models of Alzheimer's disease (AD) and PD, rTMS reduced β -amyloid levels and increased expression of neurotrophic factors like BDNF and NGF [34, 35]. Due to the non-invasive nature of rTMS and the breadth of effects relevant to ischemic stroke, this study investigated the effects of rTMS on an experimental photothrombotic (PT) rat model of ischemic stroke.

Materials and Methods

Animals and Study Design

Male Sprague-Dawley rats (200–250-g body weight) were used in the present work, and the animals were randomly divided into 3 groups: (a) healthy animals without PT stroke; (b) PT stroke animals that received sham-rTMS treatment (PT stroke control group); (c) PT stroke animals that received rTMS treatment (rTMS group). Five-minute daily rTMS treatment (initiated 3 h after PT stroke) was administered from day 0 to day 5 after PT stroke (Fig. 1b). Behavioral tests were performed from day 1 to day 13. For further analysis, rat brains were collected at day 5 (3 h after the last rTMS treatment) and day 21 after stroke induction, respectively. All the surgeries and histological counting were performed by investigators blinded to the treatment and staining groups. Randomization was used to assign groups and to collect and analyze data. Sample size (n) calculation was based on power analysis using SigmaStat 3.5 software (SPSS, Inc., IL, USA) and our previous work experience in the PT stroke model.

The predefined primary outcome measures were the reduction in infarct size and peri-infarct neuronal degeneration, functional recovery, reduction of local inflammation, and oxidative stress.

All animal procedures were approved by the Institutional Animal Care and Use Committee (IACUC) of the Augusta University (Protocol #2014-0661) and complied with the guidelines of National Institutes of Health. Every effort was made to avoid/alleviate animal pain and distress and minimize the number of animals used in the project.

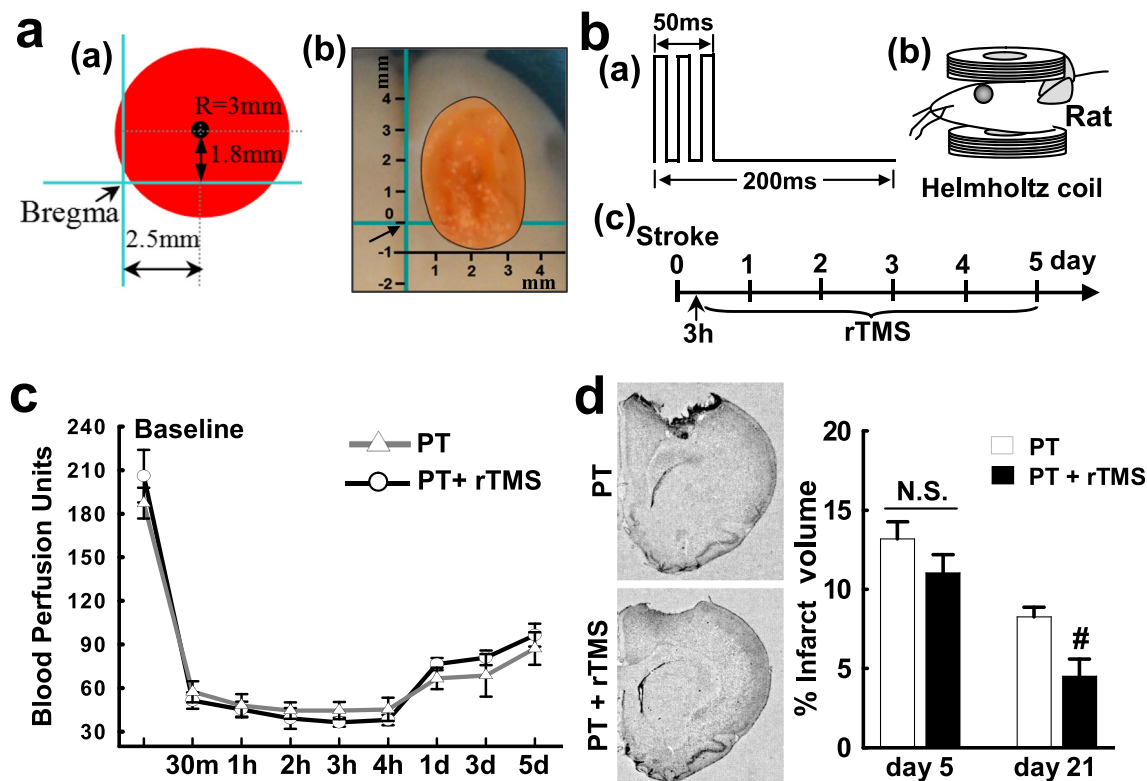


Fig. 1 PT stroke-induced cerebral infarct volume is attenuated following rTMS treatment. **a** A schematic view of the stereotaxic coordinates used to photochemically induce an ischemic infarct in the sensorimotor cortex, the area targeted by cold light (3-mm radius) is indicated by red circle (a). Diagram depicting lesion location, relative to bregma, in the rat brain 21 days after photothrombotic (PT) stroke (b). **b** Schematic illustration of a standard theta-burst stimulation paradigm (a, 3 pulses of 50 Hz repeated every 200 ms), rTMS using a Helmholtz coil (b, intensity at 200 G), and schematic diagram of the rTMS treatments (5-min daily theta-wave rTMS) from 3 h to day 5 after PT stroke (c). **c** Effects of rTMS on the regional blood flow after PT stroke. The blood perfusion

units above the infarct core were measured at the indicated time points, and the mean value versus the baseline value was defined as relative blood perfusion. Baseline blood flow values were recorded 5 min before induction of PT stroke. **d** Coronal brain sections stained with cresyl violet showing typical cortical infarcts in PT group and rTMS combination treatment group on day 21. Treatment with rTMS significantly reduces the infarct volume compared with the PT group at day 21 but not day 5 after stroke. Values are expressed as mean \pm SE ($n = 8-10$). Magnification $\times 4$ in (d); # $P < 0.05$ versus PT group without rTMS treatment. N.S., no significant difference

Photothrombotic Stroke Injury and Administration of Repetitive Transcranial Magnetic Stimulation

The rat PT stroke model was performed as previously described by our laboratory [11, 12]. In brief, the animals were intraperitoneally (i.p.) anesthetized with sodium pentobarbital (50 mg/kg) and secured in a stereotaxic frame with ear bars. The skull surface was exposed and periosteum was then gently cleaned with hydrogen peroxide, and a fiber optic cable delivering cold light (6 mm diameter) was placed stereotaxically onto the skull. Five minutes after administration of the Rose Bengal dye (0.1 mg/g of body weight, i.p.), the cleaned skull was illuminated for 15 min with the light spot centered at 1.8 mm anterior to the bregma and 2.5 mm lateral from the midline, as shown in Fig. 1 a. Rectal temperature of the animals was maintained within the range of 36.5–37.5 °C during and after surgical operation.

For rTMS treatment, a standard theta-burst stimulation paradigm (3 pulses of 50 Hz, repeated every 200 ms) of rTMS was continuously delivered to the infarct hemisphere using a pair of Helmholtz coils, as illustrated in schematic Fig. 1 b.

The wave signal and parameter were generated by an isolated pulse stimulator (model 2100, A-M system, WA, USA) and the temporal-pattern signal of amplified electromagnetic pulses was displayed and monitored using a digital oscilloscope. The intensity of the magnetic field between two coils was adjusted to 200 G, detected and monitored by using a FW Bell RoHS gauss meter (#5180, OECO LLC, OR, USA). All animals were restrained in a transparent DecapiCone (DCL-120, Braintree Scientific, MA, USA) during treatment and returned to their home cage immediately thereafter. Sham-rTMS-treated animals in PT stroke group underwent identical procedures as with rTMS-treated stroke animals except that the power of the magnetic system was not turned on.

Laser Doppler Flowmetry Monitoring

To continuously monitor the microvascular blood flow at the indicated time points (30 min, 1, 2, 3, 4 h and 1, 3, 5 d after PT stroke), the animals were anesthetized under light isoflurane

using a nose cone with the core temperature maintained at 36 °C. The skull surface was exposed and cleaned with hydrogen peroxide followed by saline. A laser OxyFlo XP Probe, which was connected to an Oxy-Lab Laser Doppler flow (LDF) Microvascular Perfusion Monitor (Oxford Optronix Ltd., UK), was vertically placed at the light-illuminated center (bregma + 1.8 mm, 2.5 mm lateral to midline). Monitoring was performed for 5 min and the collected values were recorded and averaged to provide a mean value of blood perfusion units (BPU) over the testing period. Baseline cortical blood flow was obtained by monitoring BPU before PT stroke procedures.

Brain Section Preparation and Infarct Volume Analysis

As described previously [37], under deep anesthesia with sodium pentobarbital, animals were transcatheterially perfused with ice-cold saline, followed by 4% paraformaldehyde (PFA) in 0.1 M phosphate buffer (PB). Brains were removed, post-fixed overnight with PFA, and cryoprotected with 30% sucrose until they sank. Coronal sections (25 µm each) of each rat brain were collected in series in the coronal plane of the sensorimotor cortex (~ -1 to +3 mm anterior of bregma). For calculation of relative infarct volume, every tenth section was collected and used for cresyl violet staining (~20 sections total per brain). In brief, the selected brain sections were stained with 0.01% (w/v) cresyl violet for 10 min, followed by graded ethanol dehydration.

The images of brain sections were acquired by AxioVision microscope system (Carl Zeiss, Germany). Collected images from each coronal section were imported into Image J software (NIH) and the infarct regions were traced and measured. The lesion surface area and the corresponding contralateral hemisphere area were multiplied by the depth of slice to determine the infarct volume and the contralateral side volume, respectively, for each slice. Infarct volumes from the representative slices were summed to provide a single value for each animal. The relative infarct volume in each animal was expressed as a percentage of the contralateral uninjured hemisphere [11]. A mean ± SE was calculated from the data in each group ($n = 8-10$). Statistical analysis was performed as described below.

Fluorescence Staining and Confocal Microscopy

Coronal slices (25 µm) centered on the infarction lesion were collected as above. As described in our previous study [12], the brain area of the peri-infarct regions (within 1 mm surrounding the infarct lesion) was chosen for imaging and analysis. Immunofluorescence staining was performed following the standard protocol as described in our previous study [38]. In brief, free-floating sections as prepared above were blocked with 10% normal donkey

serum for 1 h, followed by primary antibody incubation overnight at 4 °C. The following primary antibodies were used in present study: anti-Synaptophysin and Spinophilin, anti-4-HNE and 8-OHdG (Abcam); anti-MAP2, GFAP, C3d and S100A10 (Thermo Fisher Scientific); anti-Iba1 (Proteintech Group); anti-Cleaved-IL-1β, cleaved caspase-3 (Asp175) and Phospho-Histone H2A.X (Ser139) (Cell Signaling); anti-TGF-β (Santa Cruz); and anti-Malondialdehyde (MDA, Novus Biologicals). Sections were then washed three times at room temperature (RT) and incubated with appropriate Alexa Fluor donkey anti-mouse/rabbit secondary antibodies (Thermo Fisher Scientific) for 1 h at RT. After washes, the sections were mounted and coverslipped in Vectashield mounting medium with DAPI (H-1200, Vector Laboratories). To measure the changes of mitochondrial membrane potential (MMP), MitoTracker Red (MitoRed) fluorescent dye (50 ng/ml in 100 µl of saline) was administered via tail vein injection 5 min before brain collection as described [26]. The brains were then perfused with 4% PFA and post-fixed and coronal brain slices (25 µm) were prepared. After washes, the sections were mounted and sealed in Vectashield mounting medium as mentioned above.

Superoxide production in situ was detected by dihydroethidium (DHE) staining as reported in our recent work [37]. In brief, brain sections were incubated with 10 µM DHE (AnaSpec) in the dark for 10 min at RT. Sections were then washed and mounted with PBS for visualization using a confocal microscope. CellROX Green (C10444, ROS-G, Thermo Fisher Scientific) was also used for oxidative stress detection. Briefly, the reagent (5 µM in 50 µl of saline) was injected to the tail vein 5 min prior to brain collection. The brains were then perfused, fixed and sliced (25 µm) for confocal microscopy. DHE and ROS-G fluorescent intensity was analyzed and expressed as percentage changes versus contralateral (Ctl) side of PT control.

All the fluorescent images were captured under a LSM700 Meta confocal laser scanning microscope (Carl Zeiss) using ×40 oil immersion Neofluor objective. All the captured images were viewed and analyzed using LSM700 Meta imaging software or ImageJ software, and representative fluorescent images were presented.

Behavioral Tests

Neurological behavior assessments were performed to measure motor impairment and somatosensory deficits in PT stroke rats. All tests were performed in a soundproof room with a neutral environment in a blinded fashion, and recorded and analyzed using ANY-maze video tracking software (Stoelting Co., Wood Dale, IL).

Standardized batteries of behavioral tests were performed on days 1,3,5,7, and 13 after PT stroke.

These tests included:

- (a) The adhesive removal test and cylinder test, as described in our previous studies [12, 11]. Briefly, to test the changes of forepaw somatosensory activity in adhesive test, two small pieces of adhesive-backed small adhesive strips (0.35×0.45 cm) were used as bilateral tactile stimuli to the animal forelimb paws. Animals were returned to the home cages in the absence of their cagemates. Time taken to remove the adhesive tapes from forelimbs within 2 min was recorded and analyzed. The cylinder test was conducted to evaluate paw usage preference and the effect of rTMS on the asymmetry of contralateral (left) forelimb usage. Animals were placed in a transparent glass cylinder (diameter: 10 cm; height: 15 cm). During the 2-min trial, the number of contacts between left or right paws and the side of the cylinder wall was counted. The percentage of left paw usage (score % = number of left paw use/number of total paw use) was calculated and compared between groups.
- (b) The ladder dexterity test was adopted to evaluate the motor coordination after stroke using a procedure previously described [39]. A horizontal ladder rung walking test apparatus (100 cm long and 19 cm high) with metal ladder rungs (3 mm diameter) was placed 30 cm above the ground with a home cage at one end. The distance between the side walls was adjusted to 1 cm wider than an animal to prevent it from turning around. A variable irregular spacing (from 1 to 3 cm) between the rungs was changed and applied to all animals daily to minimize the animals from learning the ladder spacing pattern. Three consecutive trials were recorded daily in each animal, and the average number of missteps (missteps, slips, stumbles, and falls) was calculated and compared in the indicated days and groups.
- (c) The hanging wire test was performed to evaluate the forelimb grip strength and motor coordination, as described in our recent work [11]. A metal wire was stretched and suspended 60 cm above ground. An animal was suspended by its tail and guided to grasp the wire with the forepaws, and allowed to hang by itself without support from the tester. Hanging wire score was acquired from a 5-point scale system: 0, the animal falls off immediately; 1, the animal hangs onto the wire by two forepaws; 2, as for 1 and attempts to climb onto the wire; 3, as for 1 and uses one or both hind limbs while attempting to climb onto the wire; 4, the animal grasps the wire with all four paws, or wraps its tail around the wire. Each testing session included 3 trials with a 5-min delay interval, and the highest reading of three successive trials was selected from each animal for statistical analysis.

Brain Homogenates and Western Blotting Analysis

As described in our previous study [12], brain tissues of the peri-infarct regions from PT stroke animals and sham controls were microdissected quickly from the cortex on an ice pad and immediately frozen in liquid nitrogen. Brain homogenates and total protein fractions were prepared according to our previous protocol [38]. Protein concentrations were determined using a Modified Lowry Protein Assay kit (Pierce, Rockford, IL, USA). Western blotting was performed as described previously by our laboratory [40]. In brief, proteins (50 μ g) were separated on sodium dodecyl sulfate-poly-acrylamide gel electrophoresis (SDS-PAGE) and transferred to a PVDF membrane. The membranes were then blocked and incubated separately at 4 °C overnight with the following antibodies: anti-CD206, CD32, CD74, and CD86 (Thermo Fisher Scientific); anti-ARG1, IL-4, IL-10, iNOS, and β -actin (Proteintech Group); MnSOD (SOD2) and nitrotyrosine (3-NT) (Santa Cruz). Membranes were then washed and incubated with HRP-conjugated secondary antibodies for 1 h at RT. Bound proteins were visualized using a cold CCD digital imaging system, and semi-quantitative analyses of the bands were performed using Image J software. Band density was normalized to loading control (β -actin). Data were expressed as means \pm SE for graphical presentation and statistical analysis.

Histological Analysis

Histological examination of the brain was performed with F-Jade C and TUNEL staining using our previous procedures [38, 40]. Briefly, the collected free-floating sections (25 μ m thick) were incubated with Fluoro-Jade C (AG325, Sigma-Aldrich) working solution for 20 min in PBS as recommended by the manufacturer. Sections were washed 5 times with PBS-Triton X-100 and mounted using water-based mounting medium containing antifading agents. TUNEL labeling was performed using a Click-iT® Plus TUNEL assay kit (Thermo Fisher Scientific) following the manufacturer's protocol. All the images were obtained using a Zeiss LSM700 Meta confocal laser microscope (Carl Zeiss).

For quantitative analyses of neuronal degenerative and apoptotic cell death, the number of F-Jade C positive cells and TUNEL-positive cells per 300 \times 300 mm square in the peri-infarct cortical areas were counted in 3–5 representative brain sections from each animal. Cell counts on each of the examined sections were averaged to provide a single value for the brain. A mean \pm SE was calculated from the data in each group and compared between groups.

NADPH Oxidase Activity and Superoxide Production Assay

NADPH oxidase activity was determined as described previously by the author [38]. Photon emission from the lucigenin-chemiluminescent reaction was measured under a luminometer (PE Applied Biosystems). Relative light units (RLU) associated with NADPH oxidase activity was calculated. Superoxide anion production in the protein samples was measured as described [37]. Briefly, DHE was added to 30 μg of brain homogenate to a final concentration of 10 μM . The mixture was incubated in the dark for 10 min at RT. The fluorescence intensity was measured under a fluorescence spectrophotometer (485 nm excitation/590 nm emission). A mean \pm SE was calculated from the data collected in each group for graphical depiction.

Proteome Profiler Rat Cytokine Analysis

Cytokine array analysis was performed using the Proteome Profiler Rat Cytokine Array Panel A kit (#ARY008, R&D Systems, Inc., MN, USA) following the manufacturer's instructions. Briefly, samples from each experimental condition were pooled and 800 μg of protein per treatment group were loaded on the array's membrane. Cytokine profile was performed in duplicate and dots were detected using a chemiluminescence system as described above. The calculated average pixel density of each pair of dots, representing as relative levels of cytokines, was analyzed with ImageJ software.

Caspase Activity Assay

Caspase-9 and caspase-3 activities were measured using fluorogenic substrates as described by our laboratory [40]. In brief, the reaction was initiated by mixing the protein homogenate and substrates (Ac-DEVD-AMC for caspase-3 and Ac-LEHD-AMC for caspase-9, AnaSpec, Fremont, CA), respectively, in protease assay buffer followed by incubation for 1 h at 37 °C. The free AMC was determined on a fluorescence spectrophotometer (Perkin Elmer) with excitation at 360 nm and emission at 460 nm. Values were calculated as changes in fluorescent units per microgram of protein and presented as percentage changes compared to the sham group.

Statistical Analysis

All the data were expressed as mean \pm SE and processed by using SigmaStat 3.5 software (SPSS, Inc., IL, USA). Behavioral tests were analyzed by ANY-maze video tracking software (version 5.1, Stoelting Co.). Statistical analyses of the results were examined by one-way analysis of variance (ANOVA) or the repeated-measures ANOVA. After ANOVA, Student-Newman-Keuls' or

Dunnnett's test was used for post hoc analyses to determine differences between groups or to compare with the control group. Probability values less than 0.05 ($P < 0.05$) were considered a statistically significant difference.

Results

rTMS Treatment Attenuates PT Stroke-Induced Cerebral Infarct Volume

As indicated in Fig. 1a and d, ischemic stroke infarct of the sensorimotor cortical area was successfully induced by a classic photothrombotic method. Assessments of the changes in cerebral blood flow were carried out at the indicated time points after PT stroke. As shown in Fig. 1c, cortical blood flow, measured at the infarct center, was greatly reduced by PT ischemic insult at 30 min, 1, 2, 3, and 4 h after stroke compared to the baseline values, with slight increases over the examined time period 1, 3, and 5 days after PT stroke. There were no significant changes of relative blood perfusion between the PT stroke group and the rTMS-treated PT group. To investigate the effects of continuous theta-burst transcranial rTMS treatment initiated 3 h after PT stroke (Fig. 1b), brain sections were labeled with cresyl violet staining (Fig. 1d). Representative infarcts outlined on cresyl violet-stained brain sections and data analysis demonstrated that rTMS treatment significantly reduced infarct volume (Fig. 1c, d), at day 21 but not day 5 after stroke. The total infarct volume was reduced from $8.25 \pm 0.62\%$ in PT stroke control animals to $4.51 \pm 1.09\%$ in rTMS-treated stroke animals, representing a 45.33% reduction.

rTMS Treatment Promotes Functional Recovery

As the reduced infarct area was located at the right sensorimotor neocortex, potentially associating with primary sensory and motor function, the animals were subjected to a battery of behavioral tests on days -1 (baseline), 1, 3, 5, 7, and 13 following PT stroke. The adhesive test was conducted to compare the changes of forepaw somatosensory activity. As shown in Fig. 2a, compared with baseline of PT and sham animals, PT stroke controls spent significantly more time to remove the adhesive tape. However, on post-stroke days 5, 7, and 13, the time spent in removing adhesive tape of the rTMS-treated animals was significantly reduced compared with that of PT controls. In addition, the cylinder test was performed to test paw usage preference. The percentage of paw usage contralateral to the infarct hemisphere was calculated and compared. Data analysis revealed that the PT group animals displayed robustly decreased contralateral paw usage as compared with the baseline and sham groups (Fig. 2b).

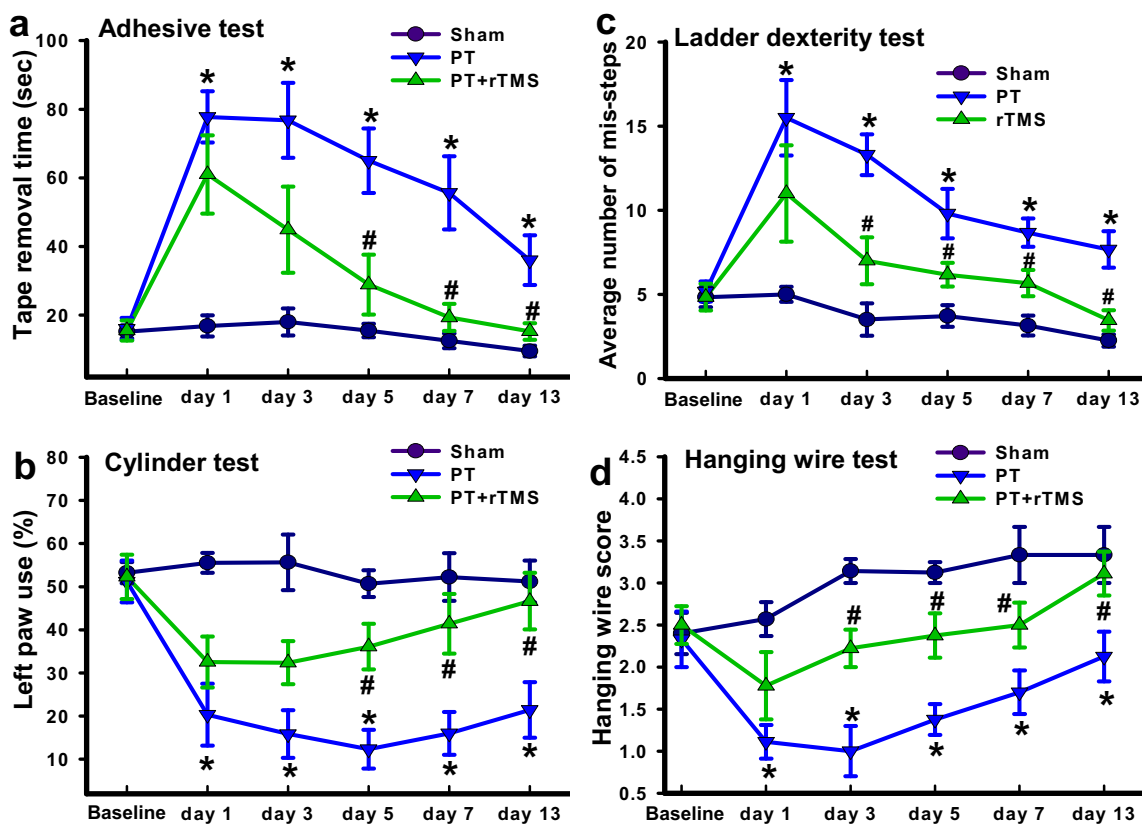


Fig. 2 rTMS treatment significantly ameliorates behavioral deficits after PT stroke. **a** The adhesive test was performed to test forepaw somatosensory activity. Time taken to remove adhesive was recorded and analyzed. **b** The cylinder test was conducted to test paw usage preference. Percentage of paw usage contralateral to the damaged hemisphere was compared between groups. **c** Motor coordination was evaluated using the ladder dexterity test. Average number of missteps

was recorded and compared in the indicated days and groups. **d** The hanging wire grip test was performed to evaluate forelimb grip strength and motor coordination. Test scores of the experimental animals were acquired from the suspended wire test. Values are expressed as mean \pm SE ($n=9-10$ /group). Baseline data was recorded 1 day before PT stroke. * $P < 0.05$ versus baseline or sham group; # $P < 0.05$ versus PT group without rTMS treatment

In contrast, the locomotor deficits in the PT group rats treated with rTMS were significantly ameliorated, as evidenced by the improved sensorimotor activity tested on post-stroke days 5, 7, and 13, compared with those of the PT control group. These behavioral improvements were further supported by the data analysis of the reduced number of missteps in the ladder dexterity test and the improved score in hanging wire grip test, on testing days 3, 5, 7, and 13 after PT stroke, demonstrating that movement coordination functions and forelimb strength were greatly improved in rTMS-treated animals (Fig. 2c, d). Taken together, these findings reveal that continuous rTMS post-treatment significantly ameliorates behavioral deficits after ischemic stroke.

rTMS Treatment Reduces PT Stroke-Induced Synaptic Loss and Neuronal Degeneration in the Peri-infarct Region

It is known that functional deficits after stroke are closely related to the loss of dendritic and synaptic proteins.

Therefore, we next investigated the effect of rTMS on dendritic and synaptic damage 5 and 21 days after PT stroke. As shown in Fig. 3a and b, representative confocal microscopy of the dendritic spine marker spinophilin (green) and the presynaptic marker synaptophysin (red) and quantitative analysis showed markedly decreased number of synaptic granules in PT stroke animals (PT vs. Ctl). Stroke animals that had rTMS post-treatment showed high density of synaptic granules (rTMS vs. PT), suggesting stroke-induced synaptic loss was prevented by rTMS post-treatment. Consistent with this interpretation, quantification of colocalized synaptic puncta revealed that rTMS-treated stroke animals exhibited increased colocalization between the signals generated by these markers in the peri-infarct region at days 5 and 21 after PT stroke, suggesting significantly preserved synaptic structure compared with PT control (Fig. 3a, b).

Correspondingly, brain sections at days 5 and 21 after PT stroke were stained with F-Jade C to explore the effects of rTMS on PT stroke-induced neuronal

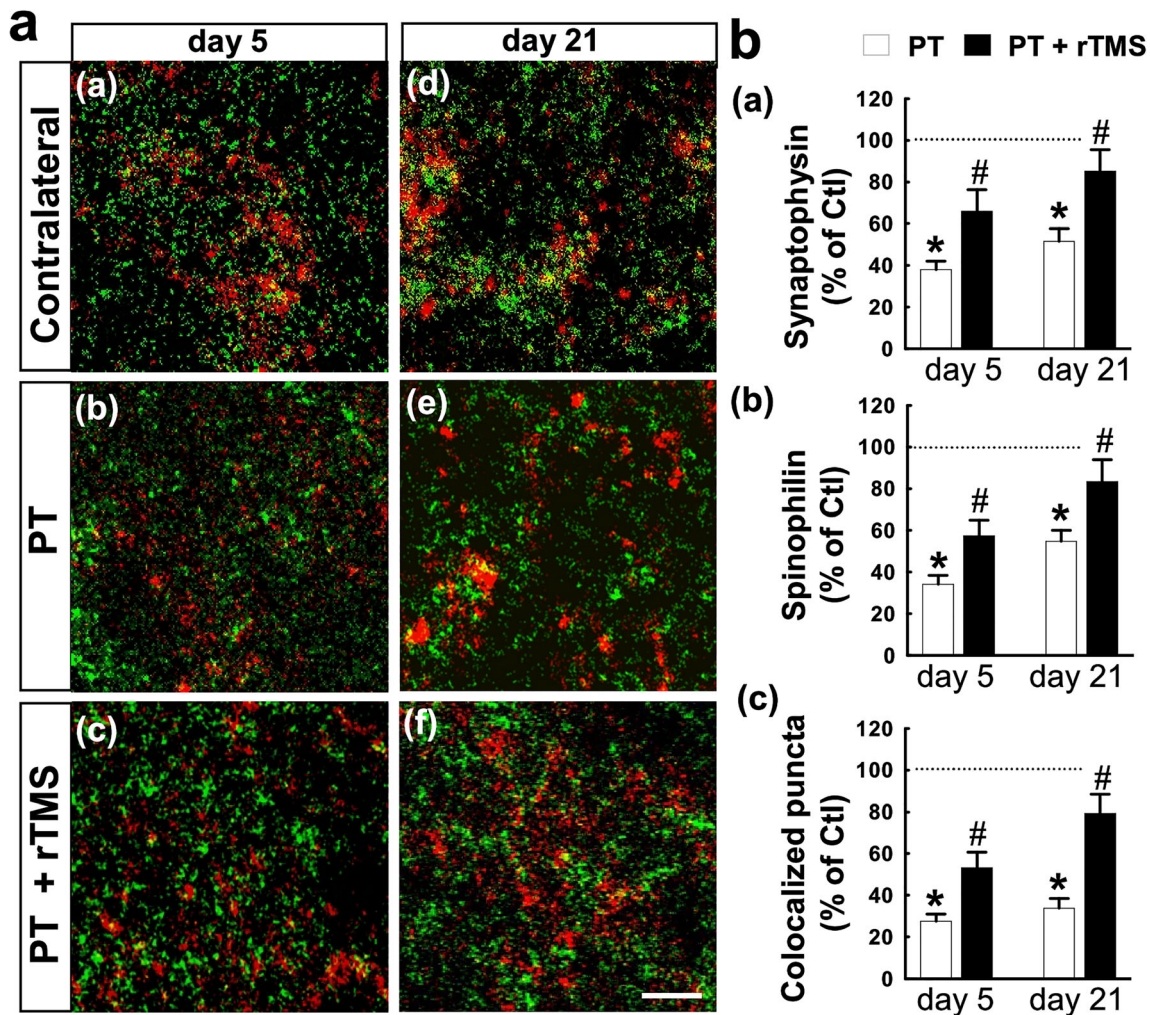


Fig. 3 rTMS treatment significantly inhibits PT stroke-induced synaptic loss. **a** Representative confocal microscopy images of the dendritic spine marker, spinophilin (green, each granule is one dendritic spine), and the presynaptic axonal bouton marker, synaptophysin (red, each granule is one axon bouton), in the peri-infarct area 5 days (a–c) and 21 days (d–f) after PT stroke. The appearance of spinophilin and synaptophysin profiles was taken from the peri-infarct region within a 1.0-mm wide belt. **b** Quantification of the number of spinophilin granules, synaptophysin

granules, and colocalized puncta between the two channels. The total number of synaptic granules and puncta per $50 \times 50 \mu\text{m}$ square were counted and quantified by using the ImageJ “Puncta Analyzer” plugin and expressed as percentage changes versus the Ctl group. Magnification $\times 120$; scale bar $10 \mu\text{m}$. Data represent mean \pm SE ($n = 6–8$). * $P < 0.05$ versus Ctl; # $P < 0.05$ versus PT group without rTMS treatment. Ctl, contralateral side

degeneration. As shown in Fig. 4 a and b, ischemic stroke resulted in significant degeneration of cortical neurons in the peri-infarct area, which was significantly ameliorated by rTMS treatment. Additionally, brain sections were labeled with MAP2, a sensitive indicator for the assessment of neuronal injury. Confocal microscopy and quantitative analysis revealed that stroke rats had less MAP2 fluorescent intensity and greater MAP2 dispersion, reflective of dendritic damage to the peri-infarct neurons. In contrast, dendritic morphology was markedly spared in stroke rats that received rTMS treatment. These data indicate that rTMS post-treatment significantly suppresses PT stroke-induced synaptic injury and neuronal degeneration in the peri-infarct region.

rTMS Treatment Reduces Microgliosis, Induces a Shift in M1/M2 Phenotype Activation, and Suppresses Pro-inflammatory Cytokines Production After PT Stroke

The expression of pro-inflammatory cytokines in the peri-infarct tissue proteins was evaluated using Proteome Profiler Rat Cytokine Array Kits. For the PT stroke control animals, we observed markedly elevated expression of 11 types secreted pro-inflammatory cytokines (CNTF, CX3CL1, IFN- γ , IL- α , IL-1 β , IL-1ra, IL-2, IL-3, IL-6, IL-17, and TNF α) compared with sham, at the day 21 time point (Fig. 5a). In contrast, the levels of these chemokines were apparently suppressed following rTMS treatment.

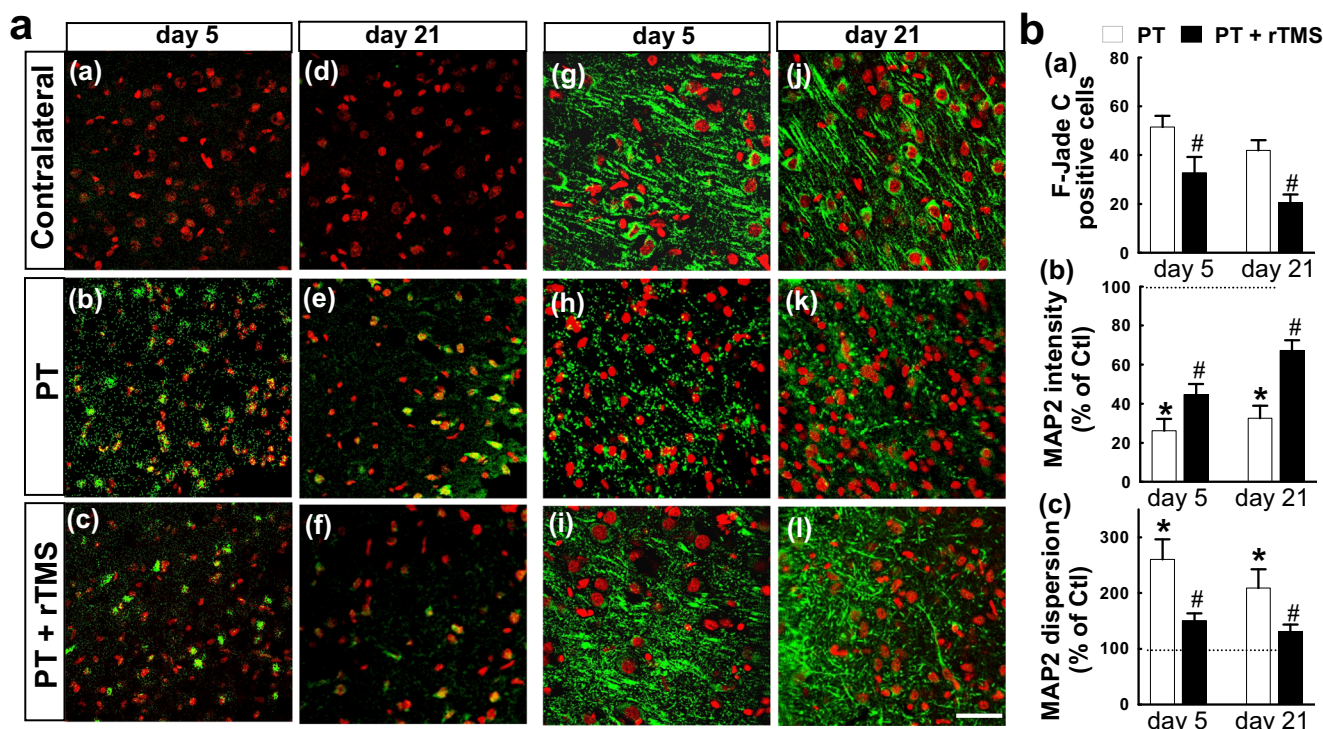


Fig. 4 rTMS treatment reduces PT stroke-induced neuronal degeneration in the peri-infarct cortical region. **a** Representative confocal microscopy images of F-Jade C staining (green in a–f) and MAP2 staining (green in g–l) in the peri-infarct cortical areas 5 and 21 days after PT stroke. Nuclei were counterstained with DAPI (native blue color was changed to red for ease of viewing). **b** Quantitative analyses of the numbers of F-Jade C

positive cells (per $300 \times 300 \mu\text{m}$ square), relative MAP2 intensity, and MAP2 dispersion 1.0 mm within the peri-infarct regions. Scale bar represents $50 \mu\text{m}$. $^*P < 0.05$ versus Ctl group; $^{\#}P < 0.05$ versus PT group without rTMS treatment. Data are presented as mean \pm SE from 6 to 8 rats in each group. Ctl, contralateral side

However, most of these measured cytokines were not very highly induced and inhibited by PT stroke and rTMS, respectively, at the early time point of day 5.

Over-activation of microglia is known to affect local inflammation, resulting in changes in the neuronal microenvironment and neuronal damage. Figure 5 b (a, f, k) shows representative confocal microscopy of Iba1 staining (green) taken from the peri-infarct region. Quantitative analyses (Fig. 5d) show robust increases in IBA1 immunoreactivity in PT stroke animals (PT vs. Ctl) and decreases in rTMS-treated animals, suggesting an effective inhibition of overall microgliosis. Additional studies in Western blotting and quantitative analyses revealed that rTMS induces a shift in M1/M2 phenotype activation, as evidenced by inhibition and elevation of levels of proteins associated with classical M1 phenotype activation (left panel in Fig. 5 c, iNOS, CD32, CD74, and CD86) and the alternative M2 phenotype activation (right panel, ARG1, CD206, IL-4, and IL-10), respectively, in the peri-infarct brain region (Fig. 5c). Immunofluorescence staining and immunoactivity intensity analyses of TGF β and CD206 further confirmed that rTMS facilitated M2 phenotype polarization (Fig. 5b, d).

As also presented in Fig. 5 band d, immunostaining for the active forms of IL-1 β (Cle-IL-1 β) and TNF α demonstrated predominant expression in the peri-infarct brain area in PT stroke animals, while these levels could be significantly reduced by rTMS post-treatment. Taken together, the results strongly support rTMS's efficacy in modulating microglia activation, reducing pro-inflammatory cytokines, and, eventually, improving the local neuronal microenvironment following ischemic stroke.

rTMS Treatment Reduces Glial Scar Formation and the Level of Reactive Astroglia and Induces an A1 to A2 Switch in Astrocytic Phenotypes After PT Stroke

Glial scar formation is one of the characteristic pathological hallmarks of stroke and a significant obstacle for stroke recovery [41]. We next explored the effects of rTMS on the profile changes of astrocytes after PT stroke, as reactive astroglia is the most important feature of glial scar formation after stroke. As presented in Fig. 6 a, the typical overview images of GFAP labeling and quantitative analyses showed a remarkable inhibitory effect of rTMS on the thickness of the glial scar.

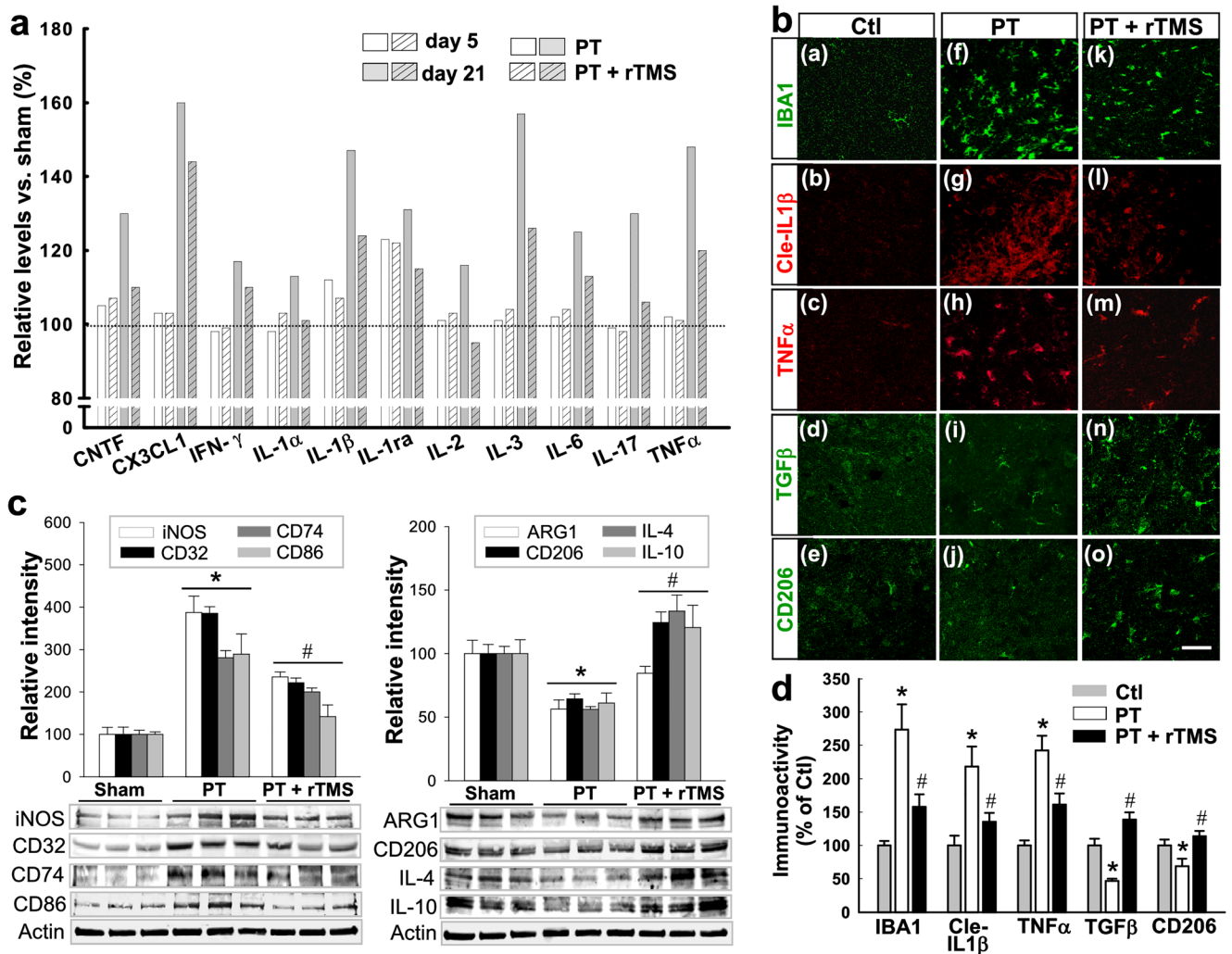


Fig. 5 rTMS treatment induces a shift in microglial M1/M2 phenotype activation and suppresses pro-inflammatory cytokine production after PT stroke. **a** The expression of inflammation-related cytokines in the tissue proteins were evaluated using Proteome Profiler Rat Cytokine Array Kits as detailed in the method. Note that expression of the indicated inflammatory cytokines was suppressed following rTMS treatment at day 21. **b**, **d** Immunofluorescence staining and immunoactivity intensity analyses of IBA1 (a marker of microglia) and the indicated inflammatory cytokines. Representative microscopy images on peri-infarct brain sections from the

Ctl, PT, and PT+rTMS groups 21 days after PT stroke are presented ($n = 5-6$ animals/group). **c** Western blotting and quantitative analyses of the indicated protein markers associated with classical activation (left panel, M1 phenotype) and alternative activation (right panel, M2 phenotype) in microglial polarization, using total protein samples from peri-infarct brain region ($n = 4-5$ animals/group). Cle-IL1β: Cleaved IL1β. Scale bar represents 50 μm. All values are expressed as mean ± SE. * $P < 0.05$ versus Ctl, # $P < 0.05$ versus PT control group without rTMS treatment. Ctl, contralateral side

Additional studies in Fig. 6 b revealed robust increases in GFAP immunoreactivity and astrocytic cell thickness within the peri-infarct cortex in PT stroke animals (PT vs. Ctl) and significant decreases in rTMS-treated stroke animals (rTMS vs. PT), respectively. Recently, reactive astrocyte phenotype heterogeneity has been noted, especially with the concept of A1 and A2 subtypes of reactive astrocytes. C3d and S100A10 staining have been used to detect both the neurotoxic “A1” phenotype and neuroprotective “A2” phenotype of astrocytes, respectively. As presented in Fig. 6 c and d, colocalization of the C3d and S100A10 signals within GFAP staining of brain astrocytes were observed, indicating astrocytic

expression of C3d and S100A10. Intriguingly, PT stroke induced significant elevated activation of A1-phenotype astrocytes compared with Ctl control, and this increase could be greatly attenuated by rTMS treatment (Fig. 6c (a–h)). Strikingly, stroke induced mild but significant activation of the protective A2-phenotype astrocytes compared with the control, and this effect was further boosted following rTMS treatment (Fig. 6d (a–h)). Taken together, our results show that rTMS post-treatment is capable of limiting PT stroke-induced glial scar formation and excessive astrogliosis, as well as switching reactive astrocytes from A1 to A2 phenotype in the peri-infarct region.

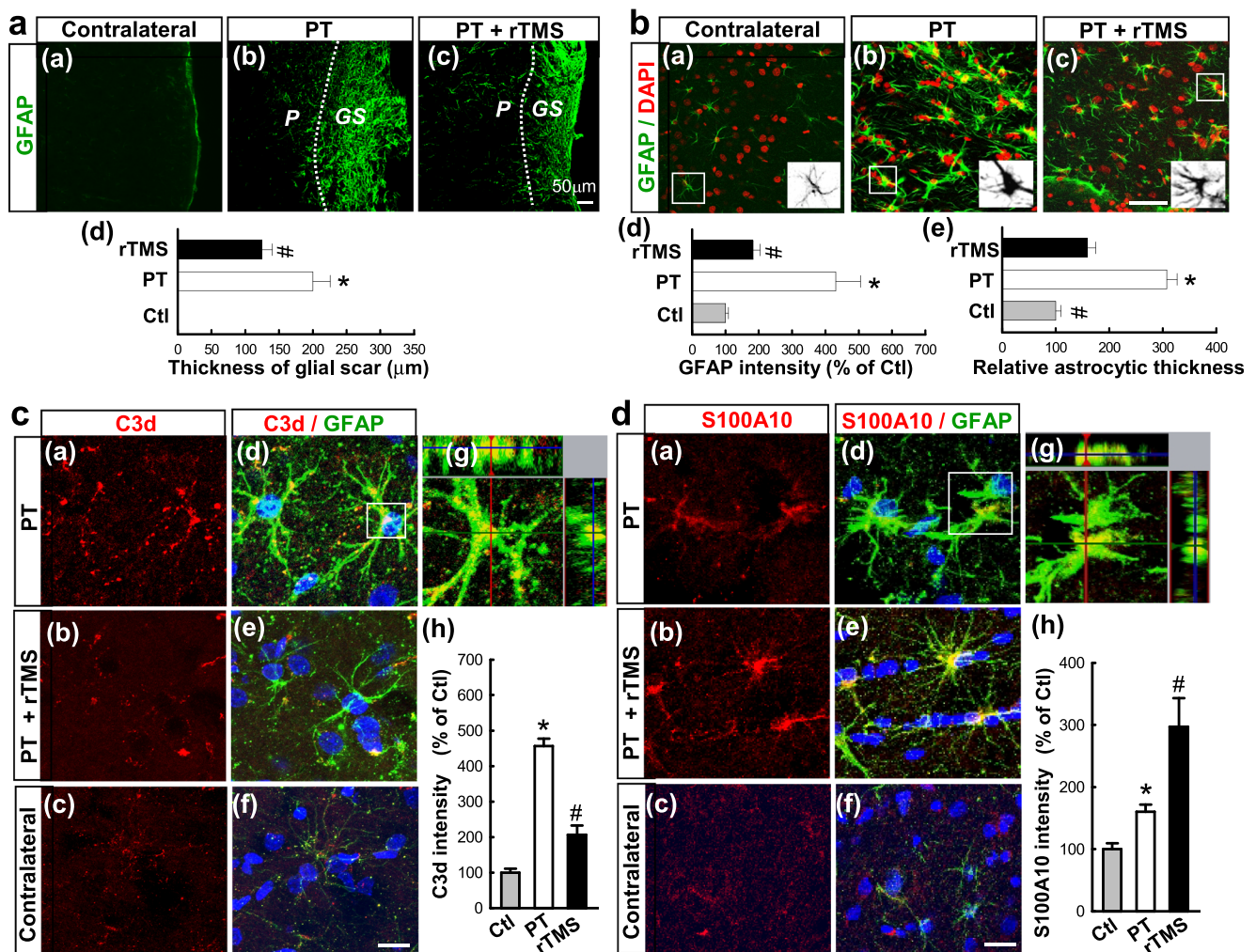


Fig. 6 rTMS treatment reduces the width of glial scar and the level of reactive astrogliosis and induces an A1 to A2 switch in astrocytic phenotypes after PT stroke. **a** GFAP fluorescence staining and the calculation of thickness of the glial scar were performed in the PT and rTMS-treated groups 21 days after stroke (Magnification $\times 10$; scale bar 50 μm ; P, peri-infarct; GS, glial scar). **b** Representative confocal microscopy images showing GFAP staining (green) and DAPI staining (red) within the peri-infarct cortex on day 21 following PT stroke (Magnification $\times 40$; scale bar 50 μm). Inserts indicate the typical morphological features of different types of astrocytes. The immunoactivity

associated with GFAP and relative astrocytic cellular thickness were quantified and compared between groups. **c, d** Representative double immunofluorescence staining and immunoactivity intensity analyses of C3d (a marker of the neurotoxic “A1” phenotype) and S100A10 (a marker of the neuroprotective “A2” phenotype) in the peri-infarct brain regions (Magnification $\times 60$, scale bar, 10 μm). Data are presented as mean \pm SE, $n = 6\text{--}8$ per group. * $P < 0.05$ versus Ctl; # $P < 0.05$ versus PT control group without rTMS treatment. Ctl, contralateral side

rTMS Treatment Reduces NADPH Oxidase Activity and Superoxide Production and Oxidative Neuronal Damage After PT Stroke

Our previous work demonstrated that activation of NADPH oxidase plays a critical role in ischemic brain damage [38, 42]. Figure 7 a reveals that NADPH oxidase activation and superoxide levels in the peri-infarct cortical proteins at days 5 and 21 after PT stroke are significantly elevated, and that these effects could be effectively attenuated following rTMS treatment. We further validated the robust induction of oxidative stress

in PT stroke rats, wherein they displayed increased DHE and ROS-G fluorescent intensity in the peri-infarct cerebral cortex (Fig. 7b), an effect that was significantly reduced by rTMS administration. Furthermore, as shown in Fig. 7 c (a–j), confocal microscopy and immunoactivity intensity analyses of oxidative damage markers were performed on brain sections 21 days after PT stroke. The results revealed that, in agreement with reduction of NADPH oxidase activity and oxidative stress by rTMS, rTMS markedly attenuated oxidative neuronal damage as measured by immunofluorescent labeling for lipid peroxidation (MDA and 4-HNE), DNA

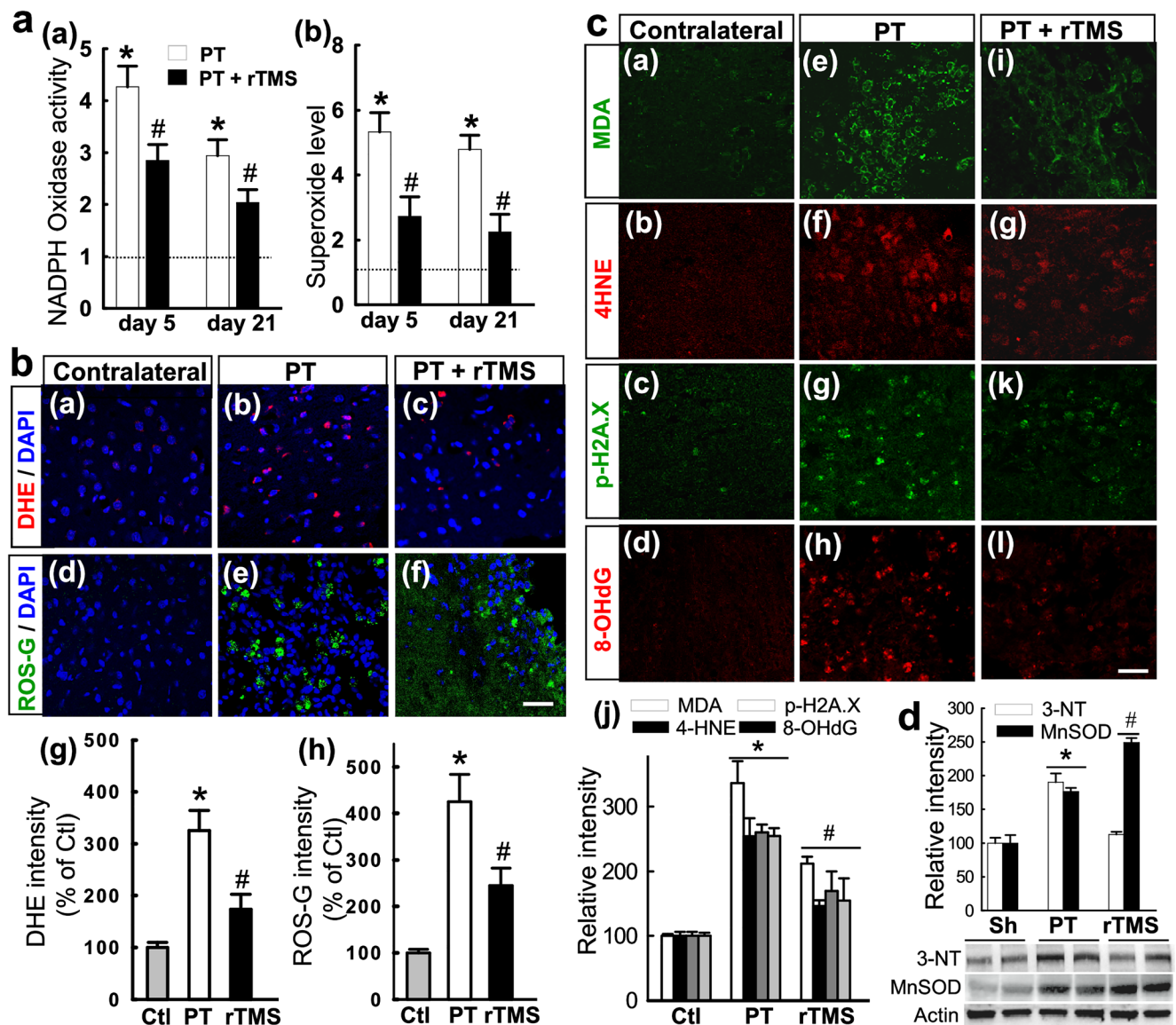


Fig. 7 rTMS treatment reduces NADPH oxidase activity and superoxide production, oxidative stress, and oxidative neuronal damage in the peri-infarct cortical region after PT stroke. **a** NADPH oxidase activity and the level of superoxide anion production, at days 5 and 21 after PT stroke, were performed using whole cell protein samples and expressed as fold increase versus sham ($n = 5-6$ per group). **b** Representative microscopy images of the peri-infarct cerebral cortex depicting dihydroethidium (DHE), ROS-G and DAPI staining at post-stroke day 21. DHE and ROS-G fluorescent intensity was analyzed using ImageJ analysis software and expressed as percentage changes versus respective Ctl control. **c** Representative Immunofluorescence staining and immunoactivity

intensity analyses of oxidative damage markers for lipid peroxidation (MDA and 4-HNE), DNA double-strand breaks (p-H2A.X Ser139), and oxidized DNA damage (8-OHdG) in the peri-infarct regions at day 21 ($n = 5-6$ per group). Fluorescence intensity was quantified using ImageJ analysis software and expressed as percentage changes versus the respective control groups. The levels of peroxynitrite production (3-nitrotyrosine, 3-NT) and the mitochondrial MnSOD isoform were explored using western blotting and quantitative analyses ($n = 4-5$ animals/group). Scale bars, 50 μm . Data are presented as mean \pm SE in each group. * $P < 0.05$ versus sham or Ctl control; # $P < 0.05$ versus PT group without rTMS treatment. Ctl, contralateral side

double-strand breaks (p-H2A.X Ser139), and oxidized DNA damage (8-OHdG). Western blotting and quantitative analyses of 3-NT (a marker for peroxynitrite production) and MnSOD isoform in total protein samples from the peri-infarct region showed that PT stroke resulted in significant increases in 3-NT and MnSOD levels compared with control groups 21 days post-

stroke (Fig. 7d). However, the elevation of 3-NT was significantly suppressed, while MnSOD production was further promoted by rTMS administration. In summary, these findings imply that rTMS post-treatment plays a novel role in attenuating oxidative neuronal damage and maintaining cellular redox homeostasis status following PT stroke.

rTMS Treatment Inhibits the Intrinsic Apoptotic Pathway and Attenuates Delayed Apoptotic Cell Death in the Peri-infarct Cortical Region After PT Stroke

We next investigated the effect of rTMS post-treatment on the activation of the intrinsic mitochondrial apoptotic pathway 21 days following PT stroke. Mitochondrial membrane potential (MMP) was assessed by evaluation of MitoRed fluorescent dye intensity in each group. As shown in Fig. 8 a (a–c and g), PT stroke induced significant collapse of MMP as reflected by MitoRed staining and fluorescence intensity analyses, suggesting the loss of mitochondrial membrane integrity. This effect was markedly abolished by rTMS administration in cortical neurons of the peri-infarct region. As demonstrated in Fig. 8 a (d–f green staining, and h), elevated immunoactivity of cleaved caspase-3 (active state) was seen in the PT stroke ipsilateral side compared with the contralateral hemisphere. Notably, rTMS exerted a robust inhibitory effect on the activation of caspase-3.

Subsequently, caspase-9 and caspase-3 activities were measured by fluorogenic substrate assay using whole cell protein samples from the peri-infarct cortex region. As shown in Fig. 8 b, rTMS dramatically prevented the increases in caspase-9 and caspase-3 activities evoked by PT stroke. Finally, the level of apoptotic neuronal death in the peri-infarct cortex region was investigated by TUNEL staining. As presented in Fig. 8 c (a–d), TUNEL staining and quantitative analyses demonstrated that rTMS treatment could markedly decrease the numbers of TUNEL-positive cells, compared with stroke control group. It should be noted that, at the time point of day 5 after stroke, we did not observe significant activation of the intrinsic mitochondrial apoptotic pathway and apoptotic cell death in the peri-infarct region (data not shown) as compared with day 21 after PT stroke. These observations suggest that post-stroke treatment of rTMS was efficient in preserving mitochondrial membrane integrity and inhibiting delayed activation of the mitochondrial/caspase apoptotic pathway following ischemic stroke.

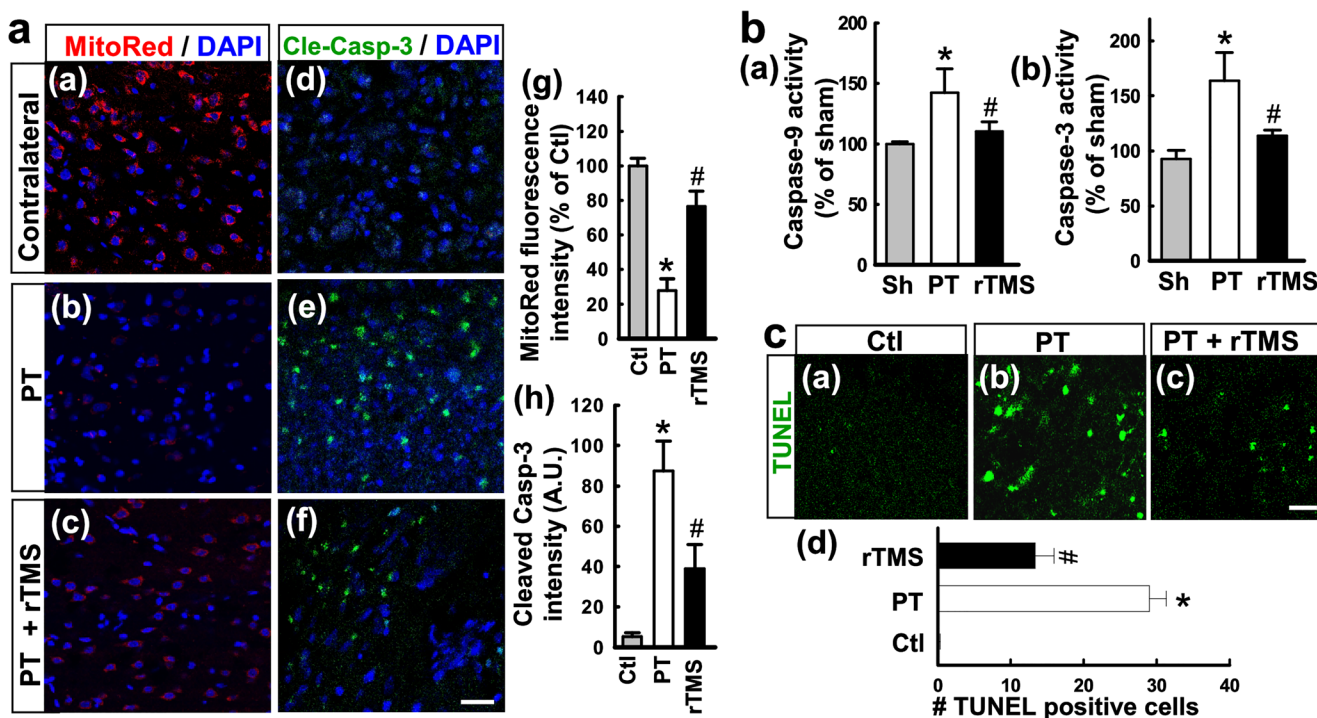


Fig. 8 rTMS treatment reduces activation of the mitochondrial/caspase apoptotic pathway in the peri-infarct cortical region after PT stroke. **a** MitoTracker Red (MitoRed) fluorescent dye was used to evaluate the changes of mitochondrial membrane integrity, and typical confocal microscopy images are shown. The mean fluorescence intensity associated with MMP in each group was further quantified as percentage changes versus Ctl. Confocal microscopy with double immunofluorescence staining for DAPI and cleaved caspase-3 (Cle-Casp-3) was performed on peri-infarct brain sections from the indicated groups 21 days after PT stroke. The level of active state of Casp-3

was evaluated by measuring its immunoactivity using Image J software. **b** Caspase-9 and caspase-3 activities were measured via a chromogenic substrate assay using whole cell protein samples, as detailed in the “Methods” section. **c** Typical fluorescent images of TUNEL staining were taken from the peri-infarct cortex region at post-stroke day 21. Quantitative analysis was performed by counting the number of TUNEL cells (per $300 \times 300 \mu\text{m}^2$ square). Scale bars $20 \mu\text{m}$. * $P < 0.05$ versus Ctl; # $P < 0.05$ versus PT group without rTMS treatment. Data are presented as means \pm SE from 6 to 8 animals in each group. A.U., arbitrary unit; Ctl, contralateral side

Discussion

The current study provides evidence that post-treatment of rTMS, initiated 3 h after a novel PT stroke model, exhibited protective properties against brain tissue loss and functional deficits induced by ischemic insult. Ischemic stroke not only induces neuronal loss in the infarct core but also synaptic dysfunction and structural damage of the surviving neurons in the surrounding peri-infarct area [7, 8]. Therefore, novel therapeutic strategies for stroke recovery have been investigated to save the affected neurons and neural circuits in the peri-infarct tissue. Accordingly, we further demonstrated that rTMS significantly reduced dendritic degeneration, synapse loss and neuronal degeneration in the peri-infarct cortical area. Importantly, the neuroprotective effects by rTMS post-treatment were correlated with the improvement of neurological recovery following PT stroke. The underlying mechanism of rTMS's neuroprotective and functional improvement applications are, at least in part, due to the multifactorial beneficial actions as elaborated in this current study: (1) reductions in excessive microglial activation by switching microglial polarization state from the toxic M1 to the protective M2 phenotype; (2) suppression of pro-inflammatory cytokine production and neuroinflammation; (3) suppression of reactive astrogliosis and glial scar formation, and induction of astrocytic phenotype activation from the neurotoxic A1 state to the neuroprotective A2 state; (4) suppression of oxidative stress and oxidative neuronal damage, at least partly, by attenuation of NADPH oxidase activity and promotion of MnSOD expression; (5) maintenance of mitochondrial membrane integrity and suppression of the intrinsic caspase-9/3 apoptotic pathway in the peri-infarct region. These key findings provide new insight into robust neuroprotective mechanisms of a novel treatment paradigm of rTMS for stroke injury that could offer neurological functional recovery for those affected by cerebral ischemia.

High-frequency (20 Hz) rTMS has been reported to restore cellular changes associated with improved functional recovery in a mouse middle cerebral artery (MCAO) model [43]. In addition, high-frequency stimulation can induce brain plasticity and cerebral blood flow increases in the primary motor cortex, which may underlie the protective mechanism rTMS's therapeutic potentials [44–46]. The short-burst and low-intensity 50-Hz rTMS is confirmed to be safe and efficient in stimulating electrophysiological and behavioral changes in the human motor cortex [47, 48]. Recently, theta-burst TMS has been used to assess pathophysiological conditions of refractory depression and AD in humans in vivo [49, 50]. While the molecular mechanisms of rTMS are currently unknown, growing evidence suggests that it can induce a robust cellular response. In a mouse PD model, rTMS application decreased brain β -amyloid levels while raising it in the cerebrospinal fluid (CSF) while simultaneously attenuating

the MKK7-ERK-Fos-APP signaling axis [34]. Applying rTMS to a mouse amyloid injection AD model, the same group found that rTMS increased levels of the neurotrophic factors and restored β -catenin signaling [35]. In both cases, these effects were accompanied by critically important functional recovery [34, 35]. A study performed on an MCAO model found rTMS upregulated expression of over 50 genes, many of which involved with cytoskeletal remodeling, inflammation, synaptic plasticity and neuroprotection [36]. In our current study, we have applied a short continuous 50 Hz theta-burst rTMS, 3 h post-stroke, targeting to the ischemic hemisphere under a Helmholtz coil, demonstrating neuronal and functional benefits. However, further studies are needed to identify the optimal stimulation protocol, doses and therapeutic window for the protective effects of theta-burst rTMS.

Pro-inflammatory cytokines are known to be released after the onset of ischemic stroke, and the resultant potent pro-inflammatory state mediates local neuroinflammation, which further contributes to neurological deterioration after cerebral ischemia. It is well documented that microglia activation is implicated in different acute neurological conditions, including stroke [15, 16]. In addition, it is conceivable that both resident microglia and peripheral monocyte-derived macrophages could be activated in the ischemia-affected tissues and contributes to the inflammation. Recent evidence suggested targeting microglia and monocytes/macrophages polarization as a novel therapeutic mechanism against stroke [17, 51]. Microglia and monocytes/macrophages polarize to the classic M1-like pro-inflammatory type (secretes pro-inflammatory cytokines) or alternative M2-like protective and reparative type (mediates anti-inflammatory effects). Thus, an important question is whether rTMS treatment could play an important role in suppressing M1 polarization and promoting M2 polarization following ischemic stroke.

Indeed, our present dataset provides critical information in this regard, as evidenced by rTMS's inhibition on the long-lasting and excessive microglial activation and the increased M1/M2 response ratio induced by PT stroke. Following activation of microglia after cerebral ischemic stroke, the release of pro-inflammatory mediators within the local neuronal microenvironment drives a chronic inflammatory response that is implicated in the pathogenesis of the ischemic cascade, leading to impaired neuron-glia communication, reduced neuronal plasticity, and cognitive impairments [52, 53]. In our present study, we found that at least 11 pro-inflammatory cytokines were remarkably elevated over control levels 21 days following PT stroke, including the CNTF, CX3CL1, IFN- γ , TNF α , and interleukin (IL) groups of cytokines. Notably, the administration of rTMS also effectively decreased the expression of multiple pro-inflammatory cytokines in the peri-infarct brain area. Intriguingly, it was shown that most of the examined inflammatory factors were not highly induced at the early stage (5-day time point) after PT stroke. This is

consistent with the evolving nature of photochemically induced stroke, wherein an inflammatory response and micro/astrogliosis are predominant features surrounding the infarct lesion 14 days after PT stroke [54]. Together, our findings support a novel efficacy of rTMS in suppressing uncontrolled and excessive activation of microglia, sustaining M2 microglial polarization and improving local microenvironment by attenuation of the release of pro-inflammatory factors following ischemic stroke.

Accumulating evidence suggest that astroglial dysfunctions contribute to the pathogenesis of neurodegenerative diseases. The glial scar is an important pathological feature after ischemic stroke in the human brain [21, 22, 55]. The formation of the glial scar physical barrier by reactive astrocytes between the peri-infarct region and the infarct core may isolate the collateral damage from diffusible and soluble factors. On the other hand, the aberrant extracellular matrix in the scar components and the morphological barrier also impedes axonal regeneration and hampers motor function recovery following stroke and traumatic brain injury [56–59]. In addition, literature has shown that inhibiting the formation of glial scarring may facilitate brain repair and neurological functional recovery [60–62]. In line with these findings, we demonstrated that rTMS has an inhibitory effect on the thickness of the glial scar after PT stroke. Concomitantly, our observations also showed that rTMS treatment markedly ameliorates stroke-induced excessive astrogliosis within the peri-infarct cortex, supporting the ability of rTMS to attenuate the dysfunction of astrocytes in ischemic pathogenesis and maintain functional neuron response.

Two astrocytic subtypes, neurotoxic A1 and neuroprotective A2-astrocytes, have been reported in the literature [20, 63]. Work from the Barres group suggests that reactive astrocytes are mainly protective in the mouse MCAO model, as they observed that A2 astrocytes expressing neurotrophic cytokines are more prominently upregulated at 1 day after 1 h-MCAO reperfusion. They also demonstrated that IL-1 α , TNF α , and C1q cytokines, derived from classical M1-type inflammatory microglia, are sufficient to induce A1 reactive astrocytes. In our present PT stroke model, both A1 and A2 astrocytes are identified by the expression of C3d and S100A10, respectively. In the expression patterns 21 days after PT stroke, A1 reactive astrocytes were 4.4-fold more highly expressed compared with the control, whereas A2 reactive astrocytes were only 1.6-fold induced in the PT stroke group. Therefore, both A1 and A2 reactive astrocyte heterogeneity have been significantly induced as tested 21 days after PT stroke, and the enlarged brain damage is associated with predominant expression of the harmful A1 phenotype at the late stroke stage in the peri-infarct region. In our study, although there was no direct evidence that confirms these A1 reactive astrocytes are induced by activated microglia, we indeed show the same activation pattern of A1/M1 and A2/M2 phenotypes,

as well as the release of the critical IL-1 α and TNF α cytokines that can induce A1 reactive astrocytes. More importantly, rTMS post-treatment could simultaneously induce a switch in microglial M1/M2 phenotype and a commensurate shift in reactive astrocytes from A1 to A2 phenotype activation. Taken together, our results strongly suggest that, rather than merely attenuating glial activation, rTMS's beneficial roles also reside in the regaining of glial balance by modulation of glial phenotypes. The glial reaction in response to rTMS therefore leads to reduced pro-inflammatory cytokines from microglia and neurotoxic function of astrocytes with an eventually improved local neuronal microenvironment following ischemic stroke.

Superoxide radical production and subsequent oxidative stress have been described as the main mechanism of brain injury caused by ischemic stroke [64–66]. It is well established that ischemia during stroke results in impaired mitochondrial respiratory chain complexes and mitochondrial dysfunction, leading to excessive production of free radicals, oxidative stress and neurodegeneration [67–69]. Excessive inflammation also induces generation of harmful free radicals that have adverse effects on neurons [70]. Superoxide dismutase (SOD) scavenger enzymes catalyze the reduction of superoxide anions to protect the cells from the damaging effects of reactive oxygen species (ROS) [71]. In mammals, MnSOD's dismutase function is to detoxify free radicals generated by mitochondrial respiration. Consistent with a previous report [72], our findings show that the level of MnSOD expression was increased in the perilesional cortex in this photothrombosis stroke model. Intriguingly, the present investigation also shows that neuroprotective amount of MnSOD was further elevated following rTMS administration, suggesting rTMS is able to activate mitochondrial antioxidant enzymes, the main endogenous protective mechanism, that significantly decrease oxidative neuronal damage after PT stroke. In addition to dysfunctional mitochondria and inflammation, recent work by our group and others demonstrate that excessive superoxide anion derived from NADPH oxidase plays a critical role in oxidative neuronal damage and functional deficits after brain ischemia [38, 42, 73–75]. In line with this evidence, the current study validated that both NADPH oxidase activity and superoxide levels in the peri-infarct cortex were highly elevated, in a prolonged manner, by PT stroke, and notably, rTMS post-treatment effectively attenuated these elevations. Our current findings, the role of rTMS post-treatment in regulating oxidative balance and attenuating oxidative neuronal damage following PT stroke, have made an important contribution and have advanced the field in the understanding of the intricate cellular mechanisms underlying rTMS's therapeutic potential in ischemic stroke.

In conclusion, our current study demonstrates that theta-burst rTMS, when initially applied on the infarct hemisphere 3 h after PT stroke, exerts profound beneficial effects

including the attenuation of cerebral infarct volume and neurodegeneration in the peri-infarct area, as well as the suppression of neurological impairment evoked by cerebral ischemic insult. The effects of rTMS post-treatment strategy appears to involve multiple mechanisms including the modulation of excessive micro/astrogliosis and glial polarizing status, improvement of the local neuronal microenvironment by balancing the homeostasis status between pro-inflammation/pro-oxidants and anti-inflammation/anti-oxidants, and the preservation of mitochondrial integrity and attenuation of mitochondrial apoptotic signaling in the peri-infarct zone. Our work also implies that a novel mechanism underlying the benefits of rTMS could result from its chronic and persistent action against the delayed apoptotic injury following stroke, especially at the late stage which is characterized by sustained activation of inflammation and oxidative stress. In summary, our findings provide evidence of the efficacy of theta-burst rTMS as a novel non-invasive transcranial therapy and a non-pharmacological therapeutic option in the management of ischemic stroke insult. Our present studies also provide important new mechanistic insights into how rTMS protects the brain after ischemic stroke, and adds additional support for the promising therapeutic effect of rTMS against neuronal injury and functional deficits following ischemic brain injury.

Acknowledgments We would like to thank Yujiao Lu for technical support with biochemical analyses.

Funding Information This study was supported by an American Heart Association Innovative Project Award 18IPA34170148 (to QZ); a Scientific Research Project of Jiangsu Provincial Commission of Health and Family Planning(Z2017016 to XZ); an Open Project Program of Jiangsu Key Laboratory of Anesthesiology (KJS1704 to XZ); and a Key Research and Development Plan of Xuzhou Science and Technology Bureau (KCI7161 to XZ).

Compliance with Ethical Standards

Conflict of Interest The authors declare that there is no conflict of interest.

Ethical Approval All procedures in studies involving animals were approved and performed in accordance with the guidelines of the Institutional Animal Care and Use Committee of the local institutes.

References

- Benjamin EJ, Muntner P, Alonso A, Bittencourt MS, Callaway CW, Carson AP, et al. Heart disease and stroke statistics–2019 update: a report from the American Heart Association. *Circulation*. 2019;139(10):e56–e528. <https://doi.org/10.1161/CIR.0000000000000659>.
- Kimani JF, Alkawi A, Panezai S, Gizzi M. Advances in thrombolytics for treatment of acute ischemic stroke. *Neurology*. 2012;79(13 Suppl 1):S119–25. <https://doi.org/10.1212/WNL.0b013e3182695882>.
- Dereck L, Cho TH. Mechanical thrombectomy in acute ischemic stroke. *Rev Neurol (Paris)*. 2017;173(3):106–13. <https://doi.org/10.1016/j.neurol.2016.06.008>.
- Akbar M, Essa MM, Daradkeh G, Abdelmegeed MA, Choi Y, Mahmood L, et al. Mitochondrial dysfunction and cell death in neurodegenerative diseases through nitroxidative stress. *Brain Res*. 2016;1637:34–55. <https://doi.org/10.1016/j.brainres.2016.02.016>.
- Ferrer I. Apoptosis: future targets for neuroprotective strategies. *Cerebrovasc Dis*. 2006;21(Suppl 2):9–20. <https://doi.org/10.1159/000091699>.
- Pekny M, Wilhelmsson U, Tatlisumak T, Pekna M. Astrocyte activation and reactive gliosis—a new target in stroke? *Neurosci Lett*. 2019;689:45–55. <https://doi.org/10.1016/j.neulet.2018.07.021>.
- Shu L, Chen B, Chen B, Xu H, Wang G, Huang Y, et al. Brain ischemic insult induces coflin rod formation leading to synaptic dysfunction in neurons. *J Cereb Blood Flow Metab*. 2018;2018:271678X18785567. <https://doi.org/10.1177/0271678X18785567>.
- Hofmeijer J, van Putten MJ. Ischemic cerebral damage: an appraisal of synaptic failure. *Stroke*. 2012;43(2):607–15. <https://doi.org/10.1161/STROKEAHA.111.632943>.
- Andrabi SS, Parvez S, Tabassum H. Progesterone induces neuroprotection following reperfusion-promoted mitochondrial dysfunction after focal cerebral ischemia in rats. *Dis Model Mech*. 2017;10(6):787–96. <https://doi.org/10.1242/dmm.025692>.
- Wang LL, Li J, Gu X, Wei L, Yu SP. Delayed treatment of 6-Bromoindirubin-3'-oxime stimulates neurogenesis and functional recovery after focal ischemic stroke in mice. *Int J Dev Neurosci*. 2017;57:77–84. <https://doi.org/10.1016/j.ijdevneu.2017.01.002>.
- Ahmed ME, Tucker D, Dong Y, Lu Y, Zhao N, Wang R, et al. Methylene Blue promotes cortical neurogenesis and ameliorates behavioral deficit after photothrombotic stroke in rats. *Neuroscience*. 2016;336:39–48. <https://doi.org/10.1016/j.neuroscience.2016.08.036>.
- Yang L, Tucker D, Dong Y, Wu C, Lu Y, Li Y, et al. Photobiomodulation therapy promotes neurogenesis by improving post-stroke local microenvironment and stimulating neuroprogenitor cells. *Exp Neurol*. 2018;299(Pt A):86–96. <https://doi.org/10.1016/j.expneurol.2017.10.013>.
- Giannakopoulou A, Lyras GA, Grigoriadis N. Long-term effects of autoimmune CNS inflammation on adult hippocampal neurogenesis. *J Neurosci Res*. 2017;95(7):1446–58. <https://doi.org/10.1002/jnr.23982>.
- Hamblin MR. Mechanisms and applications of the anti-inflammatory effects of photobiomodulation. *AIMS Biophys*. 2017;4(3):337–61. <https://doi.org/10.3934/biophys.2017.3.337>.
- Gulke E, Gelderblom M, Magnus T. Danger signals in stroke and their role on microglia activation after ischemia. *Ther Adv Neurol Disord*. 2018;11:1756286418774254. <https://doi.org/10.1177/1756286418774254>.
- Dheen ST, Kaur C, Ling EA. Microglial activation and its implications in the brain diseases. *Curr Med Chem*. 2007;14(11):1189–97.
- Zhao SC, Ma LS, Chu ZH, Xu H, Wu WQ, Liu F. Regulation of microglial activation in stroke. *Acta Pharmacol Sin*. 2017;38(4):445–58. <https://doi.org/10.1038/aps.2016.162>.
- Liu R, Liao XY, Tang JC, Pan MX, Chen SF, Lu PX, et al. BpV(pic) confers neuroprotection by inhibiting M1 microglial polarization and MCP-1 expression in rat traumatic brain injury. *Mol Immunol*. 2019;112:30–9. <https://doi.org/10.1016/j.molimm.2019.04.010>.
- Li Q, Dai Z, Cao Y, Wang L. Caspase-1 inhibition mediates neuroprotection in experimental stroke by polarizing M2 microglia/macrophage and suppressing NF-kappaB activation. *Biochem Biophys Res Commun*. 2019;513(2):479–85. <https://doi.org/10.1016/j.bbrc.2019.03.202>.

20. Liddel SA, Guttenplan KA, Clarke LE, Bennett FC, Bohlen CJ, Schirmer L, et al. Neurotoxic reactive astrocytes are induced by activated microglia. *Nature*. 2017;541(7638):481–7. <https://doi.org/10.1038/nature21029>.
21. Huang L, Wu ZB, Zhuge Q, Zheng W, Shao B, Wang B, et al. Glial scar formation occurs in the human brain after ischemic stroke. *Int J Med Sci*. 2014;11(4):344–8. <https://doi.org/10.7150/ijms.8140>.
22. Wang H, Song G, Chuang H, Chiu C, Abdelmaksoud A, Ye Y, et al. Portrait of glial scar in neurological diseases. *Int J Immunopathol Pharmacol*. 2018;31:2058738418801406. <https://doi.org/10.1177/2058738418801406>.
23. Strubakos CD, Malik M, Wider JM, Lee I, Reynolds CA, Mitsias P, et al. Non-invasive treatment with near-infrared light: a novel mechanisms-based strategy that evokes sustained reduction in brain injury after stroke. *J Cereb Blood Flow Metab*. 2019;2019:271678X19845149. <https://doi.org/10.1177/0271678X19845149>.
24. Ojo OB, Amoo ZA, Saliu IO, Olaleye MT, Farombi EO, Akinmoladun AC. Neurotherapeutic potential of kolaviron on neurotransmitter dysregulation, excitotoxicity, mitochondrial electron transport chain dysfunction and redox imbalance in 2-VO brain ischemia/reperfusion injury. *Biomed Pharmacother*. 2019;111:859–72. <https://doi.org/10.1016/j.biopha.2018.12.144>.
25. Tucker LD, Lu Y, Dong Y, Yang L, Li Y, Zhao N, et al. Photobiomodulation therapy attenuates hypoxic-ischemic injury in a neonatal rat model. *J Mol Neurosci*. 2018;65(4):514–26. <https://doi.org/10.1007/s12031-018-1121-3>.
26. Lu Q, Tucker D, Dong Y, Zhao N, Zhang Q. Neuroprotective and functional improvement effects of methylene blue in global cerebral ischemia. *Mol Neurobiol*. 2016;53(8):5344–55. <https://doi.org/10.1007/s12035-015-9455-0>.
27. Nataraj J, Manivasagam T, Thenmozhi AJ, Essa MM. Lutein protects dopaminergic neurons against MPTP-induced apoptotic death and motor dysfunction by ameliorating mitochondrial disruption and oxidative stress. *Nutr Neurosci*. 2016;19(6):237–46. <https://doi.org/10.1179/1476830515Y.0000000010>.
28. Lee Y, Park HR, Chun HJ, Lee J. Silibinin prevents dopaminergic neuronal loss in a mouse model of Parkinson's disease via mitochondrial stabilization. *J Neurosci Res*. 2015;93(5):755–65. <https://doi.org/10.1002/jnr.23544>.
29. Costa C, Tozzi A, Luchetti E, Siliquini S, Belcastro V, Tantucci M, et al. Electrophysiological actions of zonisamide on striatal neurons: selective neuroprotection against complex I mitochondrial dysfunction. *Exp Neurol*. 2010;221(1):217–24. <https://doi.org/10.1016/j.expneurol.2009.11.002>.
30. Peng Z, Zhou C, Xue S, Bai J, Yu S, Li X, et al. Mechanism of repetitive transcranial magnetic stimulation for depression. *Shanghai Arch Psychiatry*. 2018;30(2):84–92. <https://doi.org/10.11919/j.issn.1002-0829.217047>.
31. Sasaki N, Mizutani S, Kakuda W, Abo M. Comparison of the effects of high- and low-frequency repetitive transcranial magnetic stimulation on upper limb hemiparesis in the early phase of stroke. *J Stroke Cerebrovasc Dis*. 2013;22(4):413–8. <https://doi.org/10.1016/j.jstrokecerebrovasdis.2011.10.004>.
32. Siddiqi SH, Trapp NT, Shahim P, Hacker CD, Laumann TO, Kandala S, et al. Individualized connectome-targeted transcranial magnetic stimulation for neuropsychiatric sequelae of repetitive traumatic brain injury in a retired NFL player. *J Neuropsychiatry Clin Neurosci*. 2019;2019:appineuropsych18100230. <https://doi.org/10.1176/appi.neuropsych.18100230>.
33. Manor B, Greenstein PE, Davila-Perez P, Wakefield S, Zhou J, Pascual-Leone A. Repetitive transcranial magnetic stimulation in spinocerebellar ataxia: a pilot randomized controlled trial. *Front Neurol*. 2019;10:73. <https://doi.org/10.3389/fneur.2019.00073>.
34. Ba F, Zhou Y, Zhou J, Chen X. Repetitive transcranial magnetic stimulation protects mice against 6-OHDA-induced Parkinson's disease symptoms by regulating brain amyloid beta1-42 level. *Mol Cell Biochem*. 2019;458:71–8. <https://doi.org/10.1007/s11010-019-03531-w>.
35. Chen X, Chen S, Liang W, Ba F. Administration of repetitive transcranial magnetic stimulation attenuates abeta 1-42-induced Alzheimer's disease in mice by activating beta-catenin signaling. *Biomed Res Int*. 2019;2019:1431760. <https://doi.org/10.1155/2019/1431760>.
36. Ljubisavljevic MR, Javid A, Oommen J, Parekh K, Nagelkerke N, Shehab S, et al. The effects of different repetitive transcranial magnetic stimulation (rTMS) protocols on cortical gene expression in a rat model of cerebral ischemic-reperfusion injury. *PLoS One*. 2015;10(10):e0139892. <https://doi.org/10.1371/journal.pone.0139892>.
37. Zhang J, Tucker LD, Dongyan LY, Yang L, Wu C, et al. Tert-butylhydroquinone post-treatment attenuates neonatal hypoxic-ischemic brain damage in rats. *Neurochem Int*. 2018;116:1–12. <https://doi.org/10.1016/j.neuint.2018.03.004>.
38. Zhang QG, Raz L, Wang R, Han D, De Sevilla L, Yang F, et al. Estrogen attenuates ischemic oxidative damage via an estrogen receptor alpha-mediated inhibition of NADPH oxidase activation. *J Neurosci*. 2009;29(44):13823–36. <https://doi.org/10.1523/JNEUROSCI.3574-09.2009>.
39. Metz GA, Whishaw IQ. Cortical and subcortical lesions impair skilled walking in the ladder rung walking test: a new task to evaluate fore- and hindlimb stepping, placing, and co-ordination. *J Neurosci Methods*. 2002;115(2):169–79.
40. Lu Y, Wang R, Dong Y, Tucker D, Zhao N, Ahmed ME, et al. Low-level laser therapy for beta amyloid toxicity in rat hippocampus. *Neurobiol Aging*. 2017;49:165–82. <https://doi.org/10.1016/j.neurobiolaging.2016.10.003>.
41. Silver J, Miller JH. Regeneration beyond the glial scar. *Nat Rev Neurosci*. 2004;5(2):146–56. <https://doi.org/10.1038/nrn1326>.
42. Ma MW, Wang J, Zhang Q, Wang R, Dhandapani KM, Vadlamudi RK, et al. NADPH oxidase in brain injury and neurodegenerative disorders. *Mol Neurodegener*. 2017;12(1):7. <https://doi.org/10.1186/s13024-017-0150-7>.
43. Caglayan AB, Beker MC, Caglayan B, Yalcin E, Caglayan A, Yulug B, et al. Acute and post-acute neuromodulation induces stroke recovery by promoting survival signaling, neurogenesis, and pyramidal tract plasticity. *Front Cell Neurosci*. 2019;13:144. <https://doi.org/10.3389/fncel.2019.00144>.
44. Orosz A, Jann K, Wirth M, Wiest R, Dierks T, Federspiel A. Theta burst TMS increases cerebral blood flow in the primary motor cortex during motor performance as assessed by arterial spin labeling (ASL). *NeuroImage*. 2012;61(3):599–605. <https://doi.org/10.1016/j.neuroimage.2012.03.084>.
45. Gersner R, Kravetz E, Feil J, Pell G, Zangen A. Long-term effects of repetitive transcranial magnetic stimulation on markers for neuroplasticity: differential outcomes in anesthetized and awake animals. *J Neurosci*. 2011;31(20):7521–6. <https://doi.org/10.1523/JNEUROSCI.6751-10.2011>.
46. Hallett M. Transcranial magnetic stimulation and the human brain. *Nature*. 2000;406(6792):147–50. <https://doi.org/10.1038/35018000>.
47. Huang YZ, Edwards MJ, Rouin E, Bhatia KP, Rothwell JC. Theta burst stimulation of the human motor cortex. *Neuron*. 2005;45(2):201–6. <https://doi.org/10.1016/j.neuron.2004.12.033>.
48. Huang YZ, Rothwell JC. The effect of short-duration bursts of high-frequency, low-intensity transcranial magnetic stimulation on the human motor cortex. *Clin Neurophysiol*. 2004;115(5):1069–75. <https://doi.org/10.1016/j.clinph.2003.12.026>.
49. Williams NR, Sudheimer KD, Bentzley BS, Pannu J, Stimpson KH, Duvio D, et al. High-dose spaced theta-burst TMS as a rapid-acting antidepressant in highly refractory depression. *Brain*. 2018;141(3):e18. <https://doi.org/10.1093/brain/awx379>.

50. Fried PJ, Jannati A, Davila-Perez P, Pascual-Leone A. Reproducibility of single-pulse, paired-pulse, and intermittent theta-burst TMS measures in healthy aging, type-2 diabetes, and Alzheimer's disease. *Front Aging Neurosci.* 2017;9:263. <https://doi.org/10.3389/fnagi.2017.00263>.
51. Kanazawa M, Ninomiya I, Hatakeyama M, Takahashi T, Shimohata T. Microglia and monocytes/macrophages polarization reveal novel therapeutic mechanism against stroke. *Int J Mol Sci.* 2017;18(10). <https://doi.org/10.3390/ijms18102135>.
52. Kim JY, Park J, Chang JY, Kim SH, Lee JE. Inflammation after ischemic stroke: the role of leukocytes and glial cells. *Exp Neurol.* 2016;25(5):241–51. <https://doi.org/10.5607/en.2016.25.5.241>.
53. Jin R, Yang G, Li G. Inflammatory mechanisms in ischemic stroke: role of inflammatory cells. *J Leukoc Biol.* 2010;87(5):779–89. <https://doi.org/10.1189/jlb.1109766>.
54. Liu NW, Ke CC, Zhao Y, Chen YA, Chan KC, Tan DT, et al. Evolutional characterization of photochemically induced stroke in rats: a multimodality imaging and molecular biological study. *Transl Stroke Res.* 2017;8(3):244–56. <https://doi.org/10.1007/s12975-016-0512-4>.
55. Ellison JA, Velier JJ, Spera P, Jonak ZL, Wang X, Barone FC, et al. Osteopontin and its integrin receptor alpha(v)beta3 are upregulated during formation of the glial scar after focal stroke. *Stroke.* 1998;29(8):1698–706; discussion 707.
56. Yong YX, Li YM, Lian J, Luo CM, Zhong DX, Han K. Inhibitory role of lentivirus-mediated aquaporin-4 gene silencing in the formation of glial scar in a rat model of traumatic brain injury. *J Cell Biochem.* 2019;120(1):368–79. <https://doi.org/10.1002/jcb.27390>.
57. Fan YY, Nan F, Guo BL, Liao Y, Zhang MS, Guo J, et al. Effects of long-term rapamycin treatment on glial scar formation after cryogenic traumatic brain injury in mice. *Neurosci Lett.* 2018;678:68–75. <https://doi.org/10.1016/j.neulet.2018.05.002>.
58. Cai H, Ma Y, Jiang L, Mu Z, Jiang Z, Chen X, et al. Hypoxia response element-regulated MMP-9 promotes neurological recovery via glial scar degradation and angiogenesis in delayed stroke. *Mol Ther.* 2017;25(6):1448–59. <https://doi.org/10.1016/j.ymthe.2017.03.020>.
59. Hill JJ, Jin K, Mao XO, Xie L, Greenberg DA. Intracerebral chondroitinase ABC and heparan sulfate proteoglycan glypican improve outcome from chronic stroke in rats. *Proc Natl Acad Sci U S A.* 2012;109(23):9155–60. <https://doi.org/10.1073/pnas.1205697109>.
60. Li HP, Komuta Y, Kimura-Kuroda J, van Kuppevelt TH, Kawano H. Roles of chondroitin sulfate and dermatan sulfate in the formation of a lesion scar and axonal regeneration after traumatic injury of the mouse brain. *J Neurotrauma.* 2013;30(5):413–25. <https://doi.org/10.1089/neu.2012.2513>.
61. Rocamonde B, Paradells S, Barcia JM, Barcia C, Garcia Verdugo JM, Miranda M, et al. Neuroprotection of lipoic acid treatment promotes angiogenesis and reduces the glial scar formation after brain injury. *Neuroscience.* 2012;224:102–15. <https://doi.org/10.1016/j.neuroscience.2012.08.028>.
62. Huang X, Kim JM, Kong TH, Park SR, Ha Y, Kim MH, et al. GM-CSF inhibits glial scar formation and shows long-term protective effect after spinal cord injury. *J Neurol Sci.* 2009;277(1–2):87–97. <https://doi.org/10.1016/j.jns.2008.10.022>.
63. Zamanian JL, Xu L, Foo LC, Nouri N, Zhou L, Giffard RG, et al. Genomic analysis of reactive astrogliosis. *J Neurosci.* 2012;32(18):6391–410. <https://doi.org/10.1523/JNEUROSCI.6221-11.2012>.
64. Li W, Yang S. Targeting oxidative stress for the treatment of ischemic stroke: upstream and downstream therapeutic strategies. *Brain Circ.* 2016;2(4):153–63. <https://doi.org/10.4103/2394-8108.195279>.
65. Chen H, Yoshioka H, Kim GS, Jung JE, Okami N, Sakata H, et al. Oxidative stress in ischemic brain damage: mechanisms of cell death and potential molecular targets for neuroprotection. *Antioxid Redox Signal.* 2011;14(8):1505–17. <https://doi.org/10.1089/ars.2010.3576>.
66. Allen CL, Bayraktutan U. Oxidative stress and its role in the pathogenesis of ischaemic stroke. *Int J Stroke.* 2009;4(6):461–70. <https://doi.org/10.1111/j.1747-4949.2009.00387.x>.
67. Facecchia K, Fochesato LA, Ray SD, Stohs SJ, Pandey S. Oxidative toxicity in neurodegenerative diseases: role of mitochondrial dysfunction and therapeutic strategies. *J Toxicol.* 2011;2011:683728. <https://doi.org/10.1155/2011/683728>.
68. Moro MA, Almeida A, Bolanos JP, Lizasoain I. Mitochondrial respiratory chain and free radical generation in stroke. *Free Radic Biol Med.* 2005;39(10):1291–304. <https://doi.org/10.1016/j.freeradbiomed.2005.07.010>.
69. Margail I, Plotkine M, Lerouet D. Antioxidant strategies in the treatment of stroke. *Free Radic Biol Med.* 2005;39(4):429–43. <https://doi.org/10.1016/j.freeradbiomed.2005.05.003>.
70. Brown GC. Nitric oxide and neuronal death. *Nitric Oxide.* 2010;23(3):153–65. <https://doi.org/10.1016/j.niox.2010.06.001>.
71. Fridovich I. Superoxide radical and superoxide dismutases. *Annu Rev Biochem.* 1995;64:97–112. <https://doi.org/10.1146/annurev.bi.64.070195.000525>.
72. Bidmon HJ, Kato K, Schleicher A, Witte OW, Zilles K. Transient increase of manganese-superoxide dismutase in remote brain areas after focal photothrombotic cortical lesion. *Stroke.* 1998;29(1):203–10 discussion 11.
73. Yao H, Ago T, Kitazono T, Nabika T. NADPH oxidase-related pathophysiology in experimental models of stroke. *Int J Mol Sci.* 2017;18(10). <https://doi.org/10.3390/ijms18102123>.
74. Zhang QG, Wang RM, Scott E, Han D, Dong Y, Tu JY, et al. Hypersensitivity of the hippocampal CA3 region to stress-induced neurodegeneration and amyloidogenesis in a rat model of surgical menopause. *Brain.* 2013;136(Pt 5):1432–45. <https://doi.org/10.1093/brain/awt046>.
75. Raz L, Zhang QG, Zhou CF, Han D, Gulati P, Yang LC, et al. Role of Rac1 GTPase in NADPH oxidase activation and cognitive impairment following cerebral ischemia in the rat. *PLoS One.* 2010;5(9):e12606. <https://doi.org/10.1371/journal.pone.0012606>.

Publisher's Note Springer Nature remains neutral with regard to jurisdictional claims in published maps and institutional affiliations.